local surface and combined to yield the following relation for the shear stress distribution[3]

$$\frac{\tau}{\tau_w} = \frac{1}{\tau_w}\left\{\tau_w + \int_0^y \beta \frac{\partial}{\partial x}(\rho u^2)\,dy - u\beta \int_0^y \frac{\partial}{\partial x}(\rho u)\,dy - 2\int_0^y \left[\int_0^y \frac{\partial}{\partial x}(\rho u)\,dy\right] u\beta^2\kappa\,dy + \int_0^y \beta \frac{\partial p}{\partial x}\,dy\right\} \quad (1)$$

where $\beta = 1/(1+\kappa y)$ and $\tau = \mu(\partial u/\partial y) - \rho\langle u'v'\rangle$. This relation has been integrated directly using measured values of wall shear stress and tabulated profile data. Values of the partial derivatives have been determined along lines of constant mass flux using a least squares technique.

The shear stress profiles obtained are shown in Fig. 2. These profiles are consistent with the boundary condition at the wall, $d\tau/dy = dp/dx$. The trend of the shear stress profile to increase beyond the point of minimum shear stress is inconsistent with the requirement that τ approach zero in the vicinity of the edge of the boundary layer. This trend is believed to be a result of the uncertainty in determining the streamwise partial derivatives.

The trend of the maximum value of τ to increase at downstream stations has been observed in incompressible flow; however, not to the extent observed here.

The eddy viscosity and mixing length distributions were calculated using the relations

$$\frac{l}{\delta} = \frac{1}{\delta}\left(\frac{\tau}{\rho(du/dy)^2}\right)^{1/2} \quad (2)$$

$$\frac{\varepsilon}{u_\infty \delta_u} = \frac{1}{u_\infty \delta_u}\left(\frac{\tau}{\rho(du/dy)}\right) \quad (3)$$

The local value of density was obtained from the tabulated data, and the velocity derivative, du/dy, was determined by central differentiation of the velocity profile data. Examples of the mixing length distributions obtained are shown in Fig. 3. These plots exhibit a linear region near the wall with a slope of 0.65 rather than the well accepted value for zero pressure gradient flow of 0.4. Also, the peak value is seen to increase as the flow develops over the ramp model in agreement with the trend of the shear stress distribution.

The eddy viscosity distributions obtained are shown in Fig. 4. The eddy viscosity is seen to exhibit a behavior similar to that for zero pressure gradient flow with the exceptions: 1) the magnitude of the peak value is greater than that obtained for zero pressure gradient flow, and 2) the peak value increases as the flow develops over the ramp model.

The calculated distributions of mixing length and eddy viscosity for adverse pressure gradient flows have been shown to be considerably distorted when compared to their zero pressure gradient counterparts. Although velocity profiles calculated for adiabatic, nonporous walls by numerical programs exhibit only a moderate sensitivity to the eddy viscosity model employed, it is conceivable that use of the eddy viscosity models calculated here could have substantial impact.

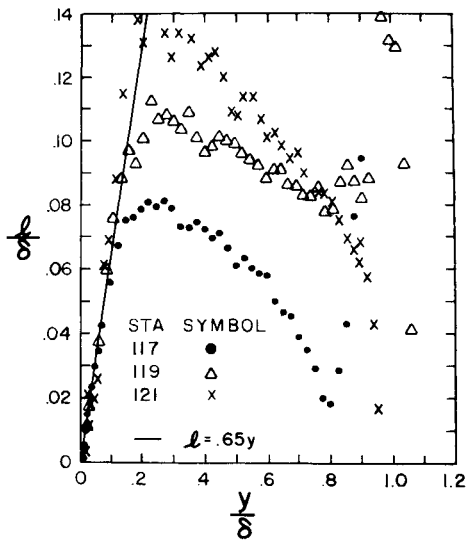

Fig. 3 Calculated mixing length distributions.

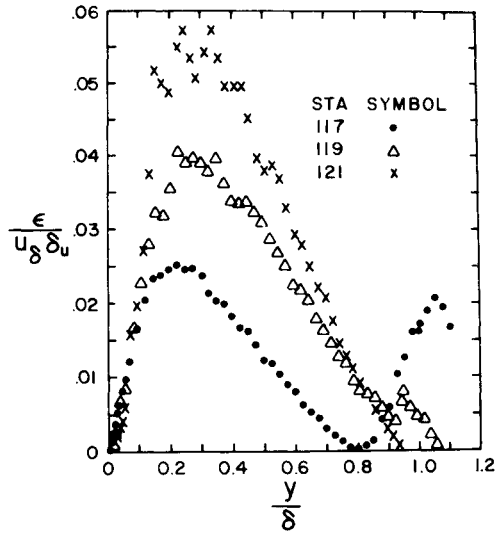

Fig. 4 Calculated eddy viscosity distributions.

References

[1] Rose, W. C., "The Behavior of a Compressible Turbulent Boundary-Layer in a Shock-Wave-Induced Adverse Pressure Gradient," Ph.D. dissertation, 1972, Univ. of Washington, Seattle, Wash.

[2] Sturek, W. B. and Danberg, J. E., "Supersonic Turbulent Boundary Layer in Adverse Pressure Gradient. Part I: The Experiment," *AIAA Journal*, Vol. 10, No. 4, April 1972, pp. 475–480.

[3] Sturek, W. B., "Calculations of Turbulent Shear Stress in Supersonic Turbulent Boundary-Layer Zero and Adverse Pressure Gradient Flow," BRL Rept. 1651, AD 763197, June 1973, U.S. Army Ballistic Research Labs., Aberdeen Proving Ground, Md.

Calculations of Flow Around a Semi-Infinite Flat Plate in a Shock Tube

TOMIKO ISHIGURO*
National Aerospace Laboratory, Chofu, Tokyo, Japan

Introduction

RECENT progress in digital computers has made the solutions of problems involving viscous compressible flows possible by means of difference methods. In this Note, we solve the case of a shock-induced unsteady laminar boundary layer on a semi-infinite flat plate without adopting the assumption[1,2] that the boundary-layer approximations are valid. In order to integrate the two-dimensional, unsteady, compressible Navier-Stokes (N-S) equations, we adopt two difference schemes; the Thommen method[3] or scheme 1 and a modified form of the Saul'ev method,[4] scheme 2, obtained by applying the Saul'ev method to the parabolic part of the N-S equations. It is found that the flowfield patterns obtained by these methods are similar,

Received April 2, 1973; revision received October 12, 1973.
Index category: Nonsteady Aerodynamics.

* Research Staff, Computation Section. Member AIAA.

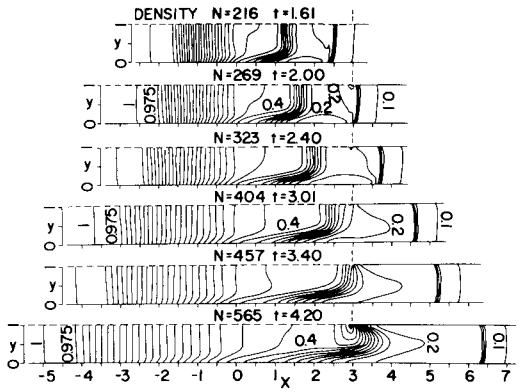

Fig. 1 Isopycnic contours showing unsteady flowfield patterns, obtained by scheme 1.

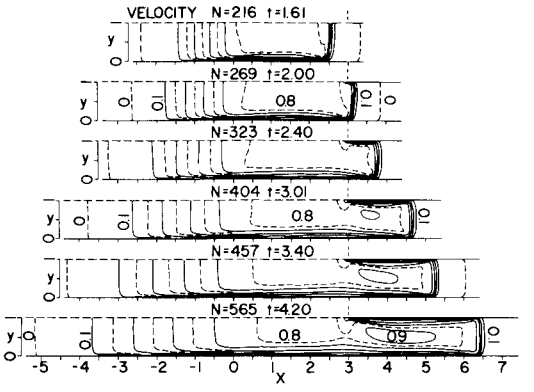

Fig. 3 Iso-velocity contours obtained by scheme 1.

qualitatively, to well-known experimental results. Numerical calculation of the preceding problem revealed that the computing time of scheme 2 is remarkably shorter than that of scheme 1, although scheme 1 gives a little better accuracy.

Difference Methods

The first scheme, scheme 1, is a combination of the Lax-Wendroff method and the central difference approximations applied to the hyperbolic and parabolic parts of the N-S equations, respectively. Since this scheme is symmetric, it can be applied to the N-S equations expressed in divergence forms with Cartesian coordinates x, y, and time t as the independent variables, and the density ρ, momentum ρu, ρv (u, v Cartesian components of the velocity vector), and the total energy per unit volume e as the dependent variables. In this Note we have assumed that the viscosity coefficient (μ) is constant and have nondimensionalized all of the quantities with the reservoir conditions [ρ_0, c_0 (sound speed) at $x = -\infty$] and the radius of the shock tube (L). Scheme 1 follows that of the Thommen method.

Next, we introduce scheme 2. We shall apply the Saul'ev method for $w_t = aw_{xx}$ ($a \geqq 0$) to the N-S equations, taking into account its unconditional stability. Since this scheme is unsymmetric, the N-S equations in the following forms:

$$V_t = -uV_x - vV_y + F(V)V_{xx} + G(V)V_{yy} + S(V_{xy}, V_x, V_y, V)$$

where V is defined as $V \equiv (\rho, u, v, T)$ (T temperature), are used because of their simple algorithm. The difference notation V_{xu} for V_x is taken as the forward difference quotient when $u < 0$, and as the backward quotient when $u \geqq 0$. We define V_{yv} in a similar way. Furthermore, we define V_{xx+} and V_{xx-} as

$$(V_{xx+})^N_{i,j} \equiv (V^N_{i-1,j} - V^N_{i,j} - V^{N+1}_{i,j} + V^{N+1}_{i+1,j})/(\Delta x)^2$$
$$(V_{xx-})^N_{i,j} \equiv (V^{N+1}_{i-1,j} - V^N_{i,j} - V^{N+1}_{i,j} + V^N_{i+1,j})/(\Delta x)^2$$

where N and (i,j) are the time cycle number and the coordinates of a node point, respectively. Likewise, V_{yy+} and V_{yy-}. From these N-S equations, scheme 2, which is effectively explicit for initial-boundary-value problems, can be constructed as a 4-step difference scheme. At each step, the terms V_t, $-uV_x$, and $-vV_y$ are approximated by the forward difference quotient, $-uV_{xu}$, and $-vV_{yv}$, respectively, and the central difference approximations are applied to the last term S. Specifically, at the first step V_{xx} and V_{yy} are approximated by V_{xx-} and V_{yy-}, at the second step by V_{xx-} and V_{yy+}, at the third step by V_{xx+} and V_{yy+}, and finally, at the fourth step by V_{xx+} and V_{yy-}, respectively.

Numerical Experiment

Placing the semi-infinite flat plate on the central line of the shock tube, the calculations are performed in the lower-half-part of the shock tube. The boundary conditions, on the adiabatic wall of the shock tube ($y = 0$) and the adiabatic semi-infinite flat plate ($x \geqq 2.98$, $y = 1$) are given as $\partial T/\partial y = 0$ and $u = v = 0$. The flow is assumed to be symmetric about the line ($x < 2.98$, $y = 1$) and the quantities, ρ, u, and e take symmetric values about this line while v takes antisymmetric values. As initial conditions ($t = 0$), $u = v = 0$ and $T = 1$ in the whole domain and $\rho = 1$ ($x \leqq 0$) and $\rho = 0.1$ ($x > 0$) are given. The ratio of specific heats γ, Prandtl number σ, and $Re \equiv \rho_0 c_0 L/\mu$ are taken to be 1.4, 0.75, and 500, respectively. (If Re is allowed to take the value, $Re = \infty$, an exact, inviscid solution of one-dimensional shock tube flow will have a shock Mach number of 1.61 under these conditions.)

The whole domain is covered with a square net according to Allen and Cheng's net covering method[5] with $\Delta x = \Delta y = 1/30$. If scheme 1 is to be used, the net should be placed so that a net line coincides with the wall. If scheme 2 is to be used, the net should be placed so that the wall lies in the midst of two neighboring net lines. Either scheme 1 or 2 can be applied to the interior points. On both the plate and the wall, the density is obtained from a difference approximation of the continuity equation while the temperature is obtained from an interpolation polynomial in y over the neighboring points, being consistent

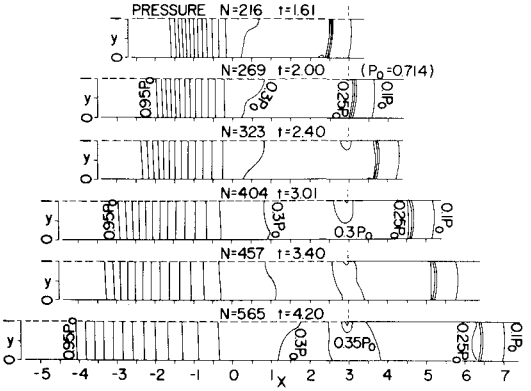

Fig. 2 Isobaric contours obtained by scheme 1.

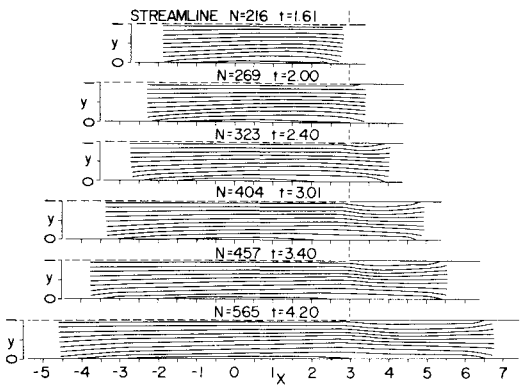

Fig. 4 Streamlines obtained by scheme 1.

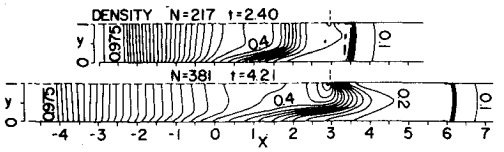

Fig. 5 Isopycnic contours obtained by scheme 2.

with the boundary conditions; for instance, on the wall when using scheme 1

$$\rho_0^{N+1} = \rho_0^N - \{4(\rho v)_1^{N+1} - (\rho v)_2^{N+1}\}\,\Delta t/(2\Delta y),$$

$$T_0^{N+1} = (4T_1^{N+1} - T_2^{N+1})/3$$

where the lower suffices 0, 1, and 2 correspond to $y = 0$, Δy, and $2\Delta y$, respectively.

A time increment when using scheme 1 is determined by the relation

$$\Delta t = 0.25\, Re\, \sigma(\Delta x)^2 \min \rho/\gamma \doteqdot 0.0074$$

which is the upper limit of the von Neumann condition for the parabolic part. The time increment when using scheme 2 is evaluated by the relation

$$\Delta t = 0.7\,\Delta x/\max(|u|+c, |v|+c)$$

which is 0.7 times that of the upper limit of the CFL condition for the hyperbolic part. (The average value of Δt obtained by this evaluation in the numerical experiment was 0.011, which was larger than the value of 0.0074 used for scheme 1. In the provisional calculation by scheme 1 with the same estimate of Δt as used for scheme 2, an instability appeared. Thus, scheme 2 is considered to be more stable than scheme 1.)

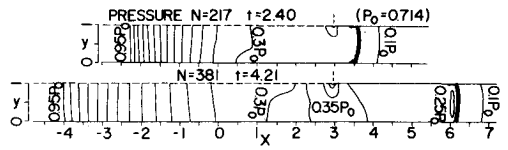

Fig. 6 Isobaric contours obtained by scheme 2.

Results

Isopycnic contours, isobaric contours, iso-velocity contours, and streamlines obtained by scheme 1 are shown in Figs. 1–4, respectively. These figures enable one to follow the unsteady flowfield patterns containing a shock wave, a contact surface, boundary layers and expansion waves numerically. For instance, at $t = 1.61$ the shock wave does not reach the leading edge of the plate, at $t = 2.00$ the shock wave just passes through the edge, at $t = 2.40$ the intermediate point between the shock wave and the contact surface passes the edge at $t = 3.01$ the contact surface reaches the edge, and at $t = 3.40$ and 4.20 complicated flowfield patterns are formed in the vicinity of the edge. These flowfield patterns are qualitatively similar to well-known experimental results. In Figs. 5–8 the isopycnic contours, isobaric contours, iso-velocity contours, and streamlines obtained by scheme 2 are shown. Comparing these with the results obtained by scheme 1, it is found that the flowfield patterns are very similar except for the fact that the shock speed is retarded a little. Since the truncation errors of scheme 1 and scheme 2 at each

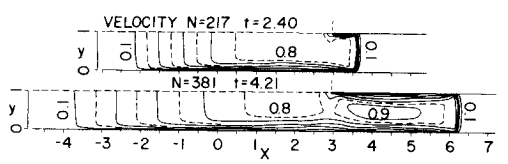

Fig. 7 Iso-velocity contours obtained by scheme 2.

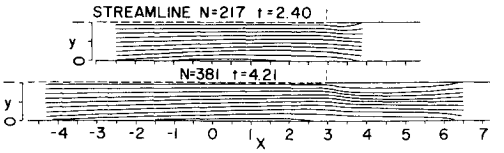

Fig. 8 Streamlines obtained by scheme 2.

step are $0(\Delta t)+0[(\Delta x)^2]$ and $0(\Delta t)+0(\Delta x)+0(\Delta t/\Delta x)$, respectively, when $\Delta x = \Delta y$, the accuracy of scheme 1 is better than that of scheme 2. Consequently, it is thought that the results obtained by scheme 1 are better than those by scheme 2.

It should be noted that the computations by scheme 1 required 230×10^{-5} sec of HITAC 5020F computer time for one time cycle and one node point, while those by scheme 2 required 98.7×10^{-5} sec. The time cycle number required up to $t = 4.2$ was 565 for the scheme 1, while only 381 for scheme 2. Consequently, the computing time of scheme 2 is shorter by a factor of 3.5 than that of scheme 1.

References

[1] Felderman, E. J., "Heat Transfer and Shear Stress in the Shock-Induced Unsteady Boundary Layer on a Flat Plate," *AIAA Journal*, Vol. 6, No. 3, March 1968, pp. 408–412.

[2] Mirels, H., "Correlation Formulas for Laminar Shock Tube Boundary Layer," *The Physics of Fluids*, Vol. 9, 1966, pp. 1265–1272.

[3] Thommen, H. U., "Numerical Integration of the Navier-Stokes Equations," *Zeitschrift für Angewandte Mathematik und Physik*, Vol. 17, 1966, pp. 369–384.

[4] Richtmyer, R. D. and Morton, K. W., *Difference Methods for Initial Value Problems*, 2nd ed., Interscience, New York, 1967, pp. 186–193.

[5] Allen, J. S. and Cheng, S. I., "Numerical Solutions of the Compressible Navier-Stokes Equations for the Laminar Near Wake," *The Physics of Fluids*, Vol. 13, 1970, pp. 37–52.

An Integral Theory for Inviscid, Rotational Flow in Variable Area Ducts

M. SAJBEN*
McDonnell Douglas Corporation, St. Louis, Mo.

A SIMPLE integral theory is presented describing the development of a class of nonuniform initial velocity profiles along a duct of variable cross-sectional area. The calculation applies to steady, incompressible, rotational flows in axisymmetric and two-dimensional passages, assuming zero viscosity. The results may serve as a crude estimate of the effects of gross initial nonuniformities for the case of relatively short ducts with insufficient length for significant boundary layer growth. The crudeness of the model is compensated for by the fact that its use requires trivial computations only, comparable to elementary manipulations of the continuity and Bernoulli equations.

Integration of the continuity equation over the duct cross section yields

$$(d/dx)(R^k \bar{u}) = 0 \qquad (1)$$

Received April 18, 1973; revision received October 19, 1973. This research was conducted under the McDonnell Douglas Independent Research and Development Program.

Index category: Nozzle and Channel Flow.

* Senior Scientist, McDonnell Douglas Research Laboratories. Member AIAA.